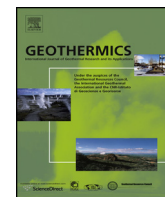




Contents lists available at ScienceDirect

Geothermics

journal homepage: www.elsevier.com/locate/geothermics



Geomechanics response and induced seismicity during gas field depletion in the Netherlands

J.D. Van Wees^{a,b,*}, L. Buijze^a, K. Van Thienen-Visser^a, M. Nepveu^a, B.B.T. Wassing^a, B. Orlic^a, P.A. Fokker^a

^a TNO, Energy Division, Utrecht, Netherlands

^b Utrecht University, Netherlands

ARTICLE INFO

Article history:

Received 24 January 2013

Received in revised form 4 April 2014

Accepted 9 May 2014

Available online xxxx

Keywords:

Induced seismicity

Gas depletion

Geomechanics

Tectonics

ABSTRACT

In this paper we present a review of controlling geological, tectonic and engineering factors for induced seismicity associated to gas depletion in the Netherlands and we place experiences from extensive Dutch geomechanical studies in the past decade in the context of generic models for induced seismicity. Netherlands is in a mature gas production phase, marked by excellent subsurface structural and stratigraphic characterization. Over 190 gas fields of varying size have been exploited. No more than 15% of these fields show seismicity. Geomechanical studies show that, similar to the EGS stimulation phase, largest seismicity is localized on pre-existing fault structures. However, the prime cause for seismicity in gas depletion is differential compaction, whereas in EGS stimulation related pressure build-up and fluid pressure diffusion along the faults form the prime mechanism. On the other hand, our study has a close theoretical analogy to reservoirs where the fluid volumes extracted are significantly larger than the re-injected volumes, and which can result in (differential) reservoir compaction.

The observed onset of induced seismicity in the Netherlands occurs after a considerable pressure drop in the gas fields. Geomechanical models show that both the delay in the onset of induced seismicity as well as the non-linear increase in seismic moment observed in the induced seismicity, can be explained using a model of differential compaction, if the faults involved in induced seismicity are not critically stressed at the onset of depletion. The presented model serves to highlight key aspects of the interaction of initial stress and differential compaction in the framework of induced seismicity in Dutch gas fields. It is not intended as predictive model for induced seismicity in a particular field. To this end, a much more detailed field specific study, taking into account the full complexity of reservoir geometry, depletion history, mechanical properties and initial stress field conditions is required.

© 2014 Elsevier Ltd. All rights reserved.

1. Introduction

From observations and theoretical models it is becoming clear that hydraulic stimulation in EGS is marked by a significant component of shear fracturing causing opening and seismicity in pre-existing fractures (Baisch et al., 2010; Kohl & Megel, 2007). Recent comparative studies have provided an excellent overview of parameters controlling the levels of seismicity in these operations (Evans et al., 2012; Shapiro et al., 2010). For individual operations, a correlation has been observed between the amount of fluid injected on one hand and the event rates and maximum magnitudes of induced events on the other (Shapiro et al., 2010). When comparing different sites, however, there appears to be a strong variability. This can be characterized by a seismogenic index, a site-dependent

offset in the Gutenberg–Richter characterization of the relationship between the event frequencies and magnitudes (Shapiro et al., 2010). It may be related to the level of natural seismicity, such as reflected by the spatial correlation of the maximum magnitudes of induced seismicity with PGA maps (Evans et al., 2012) or to the depth, as reflected by the depth dependence of maximum magnitudes as observed for shale gas stimulations (Warpinski, 2012). It has also been noted that the probability of generating seismicity is dependent on the initial stresses on the faults/fractures and their proximity to failure (Cloetingh et al., 2010; Moeck & Backers, 2011; Worum et al., 2004).

Hydraulic stimulation in EGS and gas depletion differ in many respects. Still, also in gas depletion changes in the shear and normal stress on pre-existing fractures and faults are the prime cause of seismicity (Mulders, 2003; Van Eijs et al., 2006). This implies that we can use data-based insights and physical understanding of induced seismicity in gas depletion to improve our understanding of the relationship between natural seismicity, natural stress state,

* Corresponding author at: Utrecht, Netherlands. Tel.: +31 51338919.

E-mail address: Jan.Diederik.vanWees@tno.nl (J.D. Van Wees).

fault fabric and induced seismicity in general. An earlier worldwide study on induced seismicity related to all kinds of subsurface activity (McGarr, 2002) shows a correlation of maximum magnitudes with the extent of the subsurface operations. McGarr (2002) also showed that there is a strong variability of the magnitudes on the trend line, but he did not relate these to an equivalent of the seismogenic index as Shapiro et al. (2010) proposed. However, his relationship of subarea extent with magnitude can be considered equivalent to the relationship between injected volume and maximum magnitude of events, because the injected volume can be translated to the areal extent of pressure changes in the fractures. There is a strong benefit in using findings from gas depletion to improve our understanding of induced seismicity for geothermal operations. In particular this relates to generic understanding of the control of the tectonic regime – in terms of pre-existing fault rheology and stress – on induced seismicity as well as contributing to assessing the potential effects of long term pressure depletion such as the Geysers geothermal field (Mossop and Segall, 1999; Altmann et al., 2013).

In this paper we focus on learnings from induced seismicity in gas depletion in the Netherlands. The Netherlands qualify well for such an approach for a number of reasons. In the first place, almost 200 gas fields have been developed to considerable pressure drops in the subsurface and many of them have resulted in significant induced seismicity with a maximum local magnitude $M_L = 3.5$. In terms of natural seismicity, the Netherlands is located at a transition from a seismically active area in the south toward a seismically quiescent region in the north, which experienced no tectonic earthquakes prior to gas production. The sediment structure and fault and fracture fabric is well known from over 30 years of exploration and production activities, and readily available in public datasets. Furthermore an extensive data set is available on leak off pressures providing estimates on minimum horizontal stress magnitudes.

In our approach we first introduce in Section 2 the natural stress field and the tectonic fabric. We will show that the subsurface of the Netherlands in terms of crustal stress and its fault fabric is in most parts not critically stressed, allowing relatively large pressure perturbations/stress perturbation on faults prior to the onset of failure and seismicity. Next, in Section 3, we revisit findings from an analysis of key parameters controlling induced seismicity (Van Eijs et al., 2006) extended for new data, clearly showing that induced seismicity is limited to fields which are structurally bounded or offset by steep faults. Gutenberger-Richter characteristics of the very large Groningen field, which was chosen due to its sufficient amount of seismic events to analyze temporal variations in the seismicity, consistently shows a nonlinear increase of seismic moment with pressure drop, with relative uniform b -values. Subsequently, in Section 4, the characteristics of field depletion and associated seismicity are put in a physics-based perspective based on results of geomechanical models incorporating stress field and fault structures. Geomechanical models show that both the delay in the onset of induced seismicity as well as the non-linear increase in seismic moment can be well explained in a model of differential compaction, if the faults involved in induced seismicity are not critically stressed at the onset of depletion.

2. Subsurface structure and in situ stress variability in the Netherlands

2.1. Tectonic setting

Compared to other countries in Europe the Netherlands is in a unique position as it is densely covered by exploration and production wells from the oil and gas industry. This includes over 5000 deep wells, about 60% of land coverage by 3D seismic surveys, and over 150,000 core plug measurements. In the Netherlands this data

is freely accessible at the portal of Digital Information of the Dutch Subsurface (www.dinoloket.nl) and the portal of Dutch Oil and Gas Data (www.nlog.nl). National mapping programs based on this data (TNO-NITG, 2004; Kombrink et al., 2012) provide an excellent structural characterization of the subsurface in terms of layering and faults. This mapping reveals a structure of Mesozoic and Cenozoic basin elements with sediment thickness of up to 5 km (Fig. 1).

The main tectonic events that affected the area were: (i) the Caledonian and Variscan orogenies, resulting in the assembly of the Pangea supercontinent during the Paleozoic, (ii) Mesozoic rifting, accompanying the break-up of Pangea, (iii) Alpine inversion, resulting from the collision of Africa and Europe during the Late Cretaceous and Early Tertiary, and (iv) Oligocene to recent development of the Rhine Graben rift system (Wong et al., 2007). These events have been marked by different stress fields, which repeatedly reactivated the existing faults, which were formed prior to the Mesozoic. The general structural model is, therefore, one of repeated (oblique) reactivation of basement faults which continue to control the structural grain, despite changes in tectonic regime and stress direction marked by extensional, transtensional and transpressional fault reactivation patterns; (Fig. 1). Most faults dip at angles in excess of 60° or more. Crustal scale NW-SE oriented faults bounding basement elements such as the basin border faults in Fig. 1 accommodate significantly more deformation than others, which may indicate a relative weakness deep in the crust compared to intact rock and smaller scale fault structures (Dirkzwager et al., 2000; Van Wees and Beekman, 2000).

2.2. In situ stress state in the Southern Netherlands

World Stress Map data indicate that the stress pattern of north-western Europe is presently characterized by an overall NW-SE orientation of the maximum horizontal stress σ_H , controlled by ridge push forces from the Mid-Atlantic Ridge and the collision of Africa and Europe (Grünthal and Stromeyer, 1992; Gölké & Coblenz, 1996; Heidbach et al., 2010; Plenefisch and Bonjer, 1997). The crustal stresses are sufficiently large in the south-eastern part of the Netherlands to cause significant neo-tectonic extensional deformation as reflected by differentiated Quaternary subsidence of the Roer Valley Graben and associated faulting (Cloetingh et al., 2010; Dirkzwager et al., 2000).

The Roer Valley Graben (RVG) of the southeastern Netherlands, is the locus of the highest level of observed seismicity (Fig. 1) in the Lower Rhine Graben (LRG), which forms the north eastern branch of the European Central Rift System, including the Rhine Graben toward the south (Cloetingh et al., 2010). The largest recorded earthquake in the LRG took place near Roermond 13-4-1992. It had a local magnitude of 5.8 and a moment magnitude of 5.4 (Camelbeeck, 1994). By inverting the focal mechanism data of the 1992 Roermond earthquake and its aftershocks it was found that the LRG is marked by normal faulting stress regime, for which the vertical stress is larger than the minimum and maximum horizontal stresses σ_h and σ_H , respectively and σ_H orientation is N139° (Camelbeeck, 1994; Camelbeeck & Van Eck, 1994). The confidence interval of the stress inversion on the other hand suggests that N135–165 orientations are also possible. The estimated σ_H orientation fits rather well to neo-tectonically active faults when projected to the surface, according to a fault dip of 60°. The critical ratio of shear and effective normal stress on these active faults (Worum et al., 2004) is expected to be close to the coefficient of friction to generate slip, which under the Mohr-Coulomb failure criterion is typically around 0.6 (Zoback & Townend, 2001). (Worum et al., 2004) analyzed through a slip tendency prediction for hypothetical orientation of σ_h and different magnitudes of σ_h and σ_H relative to vertical stress σ_v , which stress orientation and magnitudes gives a best fit to the observed active faults. In line with the findings

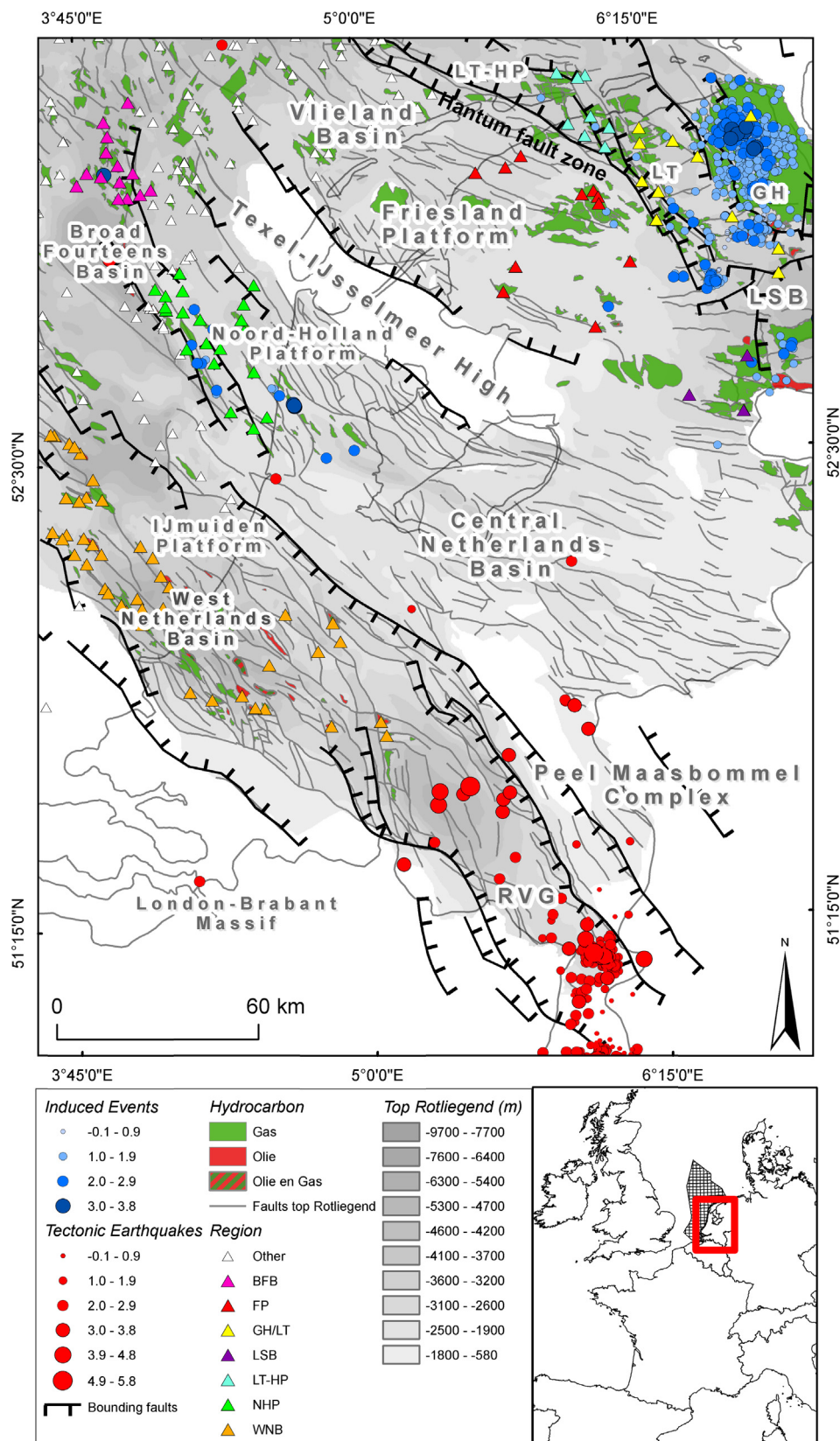


Fig. 1. Overview of tectonic elements, seismicity and hydrocarbon reservoirs in the Netherlands. Natural seismicity is shown in red circles, induced seismicity is shown in blue circles (larger events in yellow). Hydrocarbon reservoirs are indicated in green (gas) and red (oil). Major fault zones (solid lines) separate the main tectonic elements which characterize the subsurface of the Netherlands (after Wong et al., 2007). Triangles correspond to Leak off test (LOT) data in Fig. 2. Colors denote different regions: BFB = Broad Fourteen Basin, FP = Friesland Platform, GH/LT = Groningen High/Lauwerszee Trough, LSB = Lower Saxony Basin, LT-HP = Lauwerszee trough-Hantum Platform, NHP = Noord Holland Platform, WNB = West Netherlands Basin. RVG = Roer Valley Graben, PB = Peelrand Block, EL = Ems Low.

Source: KNMI (2012) seismic catalog, NLOG (2012) for depth of top Rotliegend, gasfields and faults). (For interpretation of the references to color in this figure legend, the reader is referred to the web version of the article.)

from the focal mechanisms, it was concluded that the maximum principal stress of the stress field in the LRG is more likely vertical (normal faulting regime) than horizontal. In terms of stress orientation Worum et al. found that the N145E orientation of σ_H in the LRG results in slightly higher slip tendency values than a N160E orientation, favoring the first scenario.

In summary the in situ stress state in the south-east Netherlands favors normal faulting with $\sigma_v > \sigma_H > \sigma_h$, with a σ_H orientation of 145–160°. The σ_v magnitude increases with burial depth, which is estimated for the sedimentary infill in the Netherlands at 2.2 bars/10 m (e.g. Hofstee et al., 2009). The σ_h magnitude can be determined from the assumption that faults are critically stressed. For optimally oriented faults in a stress field where the maximum principal stress is the vertical stress σ_v , we can estimate the ratio of the effective stress ratio as $K' = \sigma'_h / \sigma'_v$ which should prevail to generate slip and earthquakes on favorably oriented faults (Jaeger and Cook, 1969; Byerlee, 1978):

$$K'_\mu = \frac{1}{(\sqrt{(\mu^2 + 1) + \mu})^2} \quad (1)$$

where μ is the coefficient of friction. For a coefficient of friction of 0.6, $K'_{\mu=0.6}$ equals 0.32 at the frictional limit. For a hydrostatic pore pressure gradient of 1 bar/10 m the σ_h magnitude is such that $K' = K'_{\mu=0.6}$, is equal to ca. 1.4 bar/10 m.

2.3. In situ stress in the northern Netherlands

The subsurface of the northern Netherlands is characterized by different basin compartments including the Groningen High (GH), Lauwerszee Through (LT), Friesland Platform (FP) (Fig. 1), which has been tectonically inactive since Cenozoic. This agrees with the fact that no natural seismicity has been recorded in recent history. For the period prior to the first induced event in 1986 in Assen (Eck et al., 2006) we have no hard evidence of any tectonic events in the North of the country. Further, all current seismicity in the north of The Netherlands (Fig. 1) recorded with instrumentation installed after 1986 occurred at a 'shallow' depth. Most events have been located around a depth of 2.5 km. No events occurred at depths larger than 4 km and all events have so far been located in or around exploited gas fields. Consequently, it was concluded that all the registered seismicity is induced by gas exploitation (Eck et al., 2006).

The absence of natural seismicity and active faulting strongly suggests that the stress field is less critical in the northern Netherlands, than in the south. Borehole breakout analysis carried out in the NE Netherlands indicated a $N160 \pm 5\sigma_H$ orientation (Frikken, 1996; Rondeel & Everaars, 1993). In the offshore of the Netherlands similar variations have been observed which have been attributed to some degree to differences in overpressures and lithology (Breckels and Van Eckelen, 1982; Verweij et al., 2012). The onshore corresponds to normal hydrostatic pressure gradient in the south up to a slightly overpressured gradient up to 1.2 bar/10 m in the north (Hofstee et al., 2009; NAM, 2010).

Furthermore, leak-off tests (LOTs) are available to estimate σ_h magnitudes. The depth trend of σ_h from public data (NLOG, 2012) has been plotted in Fig. 2. The data are grouped per region based on structural elements defined in the Netherlands (Fig. 1), and where applicable their vicinity to hydrocarbon fields exhibiting seismicity. For σ_v an average overburden pressure of 2.2 bar/10 m was assumed. The vast majority of these measurements have been taken prior to reservoir production.

To obtain the effective stress ratio K' , the effective stresses σ'_h and σ'_v were constructed by subtracting estimated pressure (Terzaghi, 1943). Pore pressures in the Netherlands may be above the hydrostatic pore pressure as some formations are

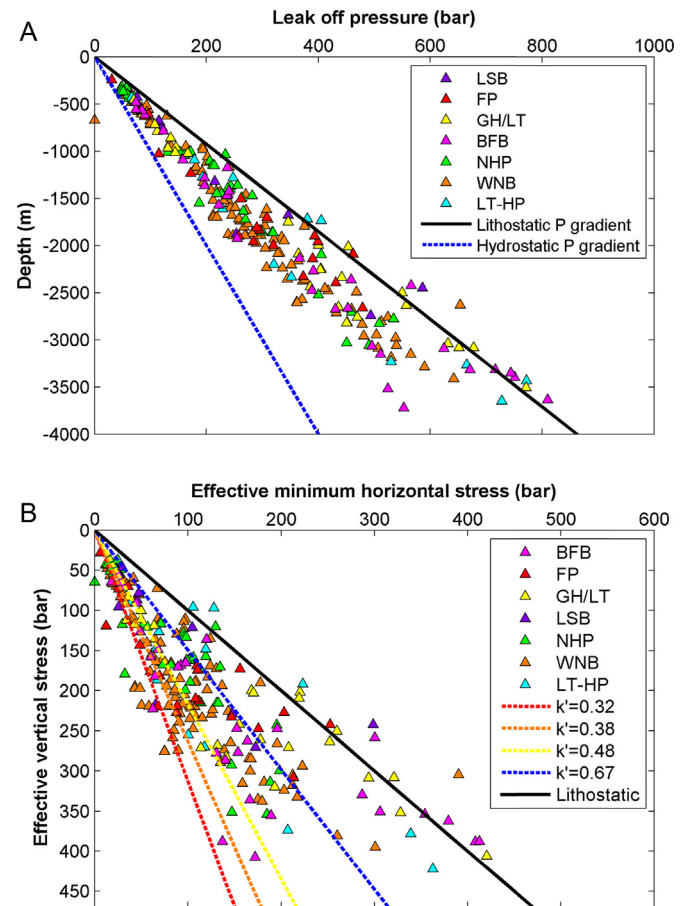


Fig. 2. Leak off pressure test (LOT) data from the onshore Netherlands (for location see Fig. 1). (A) Measured leak off pressures and hydrostatic gradient (1 bar/10 m) and lithostatic (2.2bars/10 m) gradients, (B) Effective minimum horizontal and vertical stress $\sigma'_h = \sigma_h - p$ and $\sigma'_v = \sigma_v - p$. These have been calculated from the leak off pressures, interpreting leak off pressures as σ_h , taking lithostatic stress for σ_v and correcting for pressure through subtracting estimated (over)pressure p following Terzaghi's concept (Terzaghi, 1943).

overpressured (Verweij et al., 2012), sometimes quite far. It is thus important to get an independent measure of the pressure. Where available, the (over)pressure was taken from pressure data in the same well in which the Leak off pressure was measured, available online (www.nlog.nl). If no pressure measurement was available, the average overpressure in a stratigraphic group was estimated from Verweij et al. (2012). Where no data was available, hydrostatic pore pressure was assumed.

Fig. 2b shows partly relatively critical stress conditions for the shallow reservoirs up to 2 km depth located in the (south) west. In particular in the West Netherlands Basin (WNB) and Noord Holland Platform (NHP) regions, a significant portion of the data indicate close to critically stressed normal faulting conditions. This agrees with earlier findings in the WNB in Barendrecht (NAM, 2010). In the north-east in the Friesland Platform (FP), Groningen High and Lauwerszee Trough (GH/LT) the leak off pressures mostly indicate relatively stable stresses up to large depth. The inferred non-critical σ_h in the north east, assuming a friction coefficient of 0.6 (corresponding to a critical $K' = 0.32$), agrees with earlier findings for the Friesland Platform (Hofstee et al., 2009), and the offshore, where LOTs also indicate non-critical σ_h magnitudes (e.g. Breckels and Van Eckelen, 1982). It should be noted that considerable stress heterogeneities in σ_h with depth are observed. This may to some degree be attributed to the lack of information on formation overpressure. For example for the Broad Fourteens Basin currently no high overpressures are assumed, whereas in some cases the Zechstein formation

may be severely overpressured (Verweij et al., 2012), which may cause the deep BFB σ_h' data in Fig. 2 to shift more toward lithostatic, i.e. $\sigma_h' = \sigma_v'$. In summary, the leak off test data and absence of historical natural seismicity in the north(-east) of the Netherlands jointly indicate that the crust is less critically stressed in the north(-east) as compared to the south(-west). These high σ_h' magnitudes from leak off test agree with findings from leak-off test in other tectonically quiescent regions, where maximum and minimum stresses have also been proved to be closer to lithostatic state compared to tectonically active areas (Fjaer et al., 1993).

3. Induced seismicity and geomechanics characteristics of gas depletion

Since the discovery of the Groningen Gas Field in 1959, gas production has been ongoing in the north of the Netherlands. After the first induced seismicity event, observed in 1986, gas-production-induced seismicity has become a growing problem in the Netherlands. From 1989 on, induced seismic events have also been registered near gas fields in the north-west of the Netherlands near Purmerend and Alkmaar.

A more sensitive seismic network, with a magnitude of completeness of 1.5, was installed by the Royal Dutch Meteorological Institute (KNMI) in 1995. Until August 2012, more than 800 events have been recorded; a catalog of induced events can be retrieved from the website of the Royal Dutch Meteorological Institute (www.knmi.nl). Local magnitudes on the Richter scale range from $M_L = -0.75$ to $M_L = 3.5$.

The induced seismic events are relatively small in magnitude. The $M_L = 3.5$ events occurred 9th September 2001 near the city of Alkmaar and 8th August 2006 near Westeremden (Groningen). Induced seismicity has generally led to slight damage on buildings, such as damaged plaster, small cracks and the widening of existing cracks (Eck et al., 2006). The last seismic event ($M_L = 3.4$) in the study presented here, took place in Huizinge in the Groningen gas field August 16th 2012 and caused considerably more damage than any of the other events.

In Fig. 3 we plotted for all gas fields the magnitudes of events registered until August 2012 as a function of pressure drop in the reservoirs, based on data from Van Thienen-Visser et al. (2012) and NAM (2010). Markedly all gas fields show a delay in the occurrence of induced seismicity, taking at least 28% of relative pressure drop prior to the onset of seismicity. Furthermore, the relationship of relative depletion with magnitudes is characterized by an upper bound which shows a trend of increasing maximum magnitudes with DP/P_{ini} .

The largest and best documented gas field in the Netherlands is the very large Groningen Gas Field, located on the Groningen High. Due to the abundance of seismic events, the statistical relationships of observed seismicity can be applied for this field. The seismicity displayed in Fig. 4 clearly shows a growing trend in the number of events and maximum magnitude with production time. This relation is similar as shown in Fig. 3, as for the Groningen Field the cumulative production and associated pressure drop is behaving approximately linear over the considered time window, and the pressure drop shows little variation in the field, as the hydraulic transmissivity in the field is excellent (NAM, 2010; Muntendam-Bos and De Waal, 2013). In Fig. 4, the cumulative seismic moment has been calculated from the sum of Seismic moment M_0 of each event adopting the relationship from (Aki, 1966; Hanks & Kanamori, 1979):

$$M_L = \frac{2}{3} \log M_0 - 6.07 \quad (2)$$

The cumulative seismic moment is marked with a strongly non-linear increase with production time and pressure drop.

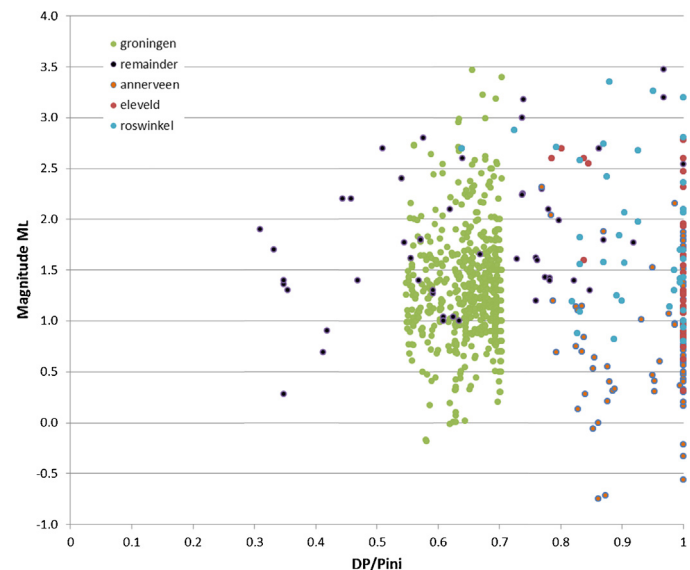


Fig. 3. local magnitudes M_L of induced events in the Netherlands as a function of depletion pressure. For each field, the depletion parameter (DP/P_{ini}) has been constructed for each earthquake from a linear interpolation of initial pressure to pressures reported at the time of first earthquake (Van Thienen-Visser et al., 2012) and pressures reported in the NAM report on subsidence evolution (NAM, 2010). The large number of points plotted at $DP/P_{ini} = 1$ for Eleveld and Rosinkel, is most likely an artifact of the interpretation of the linear trend – in the progressive decrease of pressure drop after the onset of the first earthquake.

The number of earthquakes in most fields is insufficient to determine Gutenberg-Richter (GR) characteristics:

$$\log(N) = a - bm \quad (3)$$

where N is the number of events larger than magnitude m . An exception is the Groningen Gas Field, in which ~600 events have been recorded. We analyzed the a - and b -values of the Groningen Field with a maximum likelihood fit using the program ZMAP (Wiemer, 2001). The magnitude of completeness was fixed at $M_x = 1.5$, which is the recording threshold of the monitoring system since 1995 up to the present date (Dost et al., 2012). Errors were computed with a bootstrapping method. Events from 1996 to 2013 are taken into account. To study the behavior of the a -value and b -value with time, a moving time window containing 60–150 events was used for the calculations. For each calculation the window was shifted in time 1 year. In the first time period the window size was 10 years, at the end of the time period the time window size was reduced to be able to capture the earthquake statistics in the last few years. Since the field became more active, the number of events in the time windows stayed roughly the same, despite their becoming shorter. Fig. 5 shows a -values and b -values derived from the Groningen field data with the center of the time window indicated at the x-axis. a values increase progressively (monotonically) with time from a value of about 2.4 in 2001 to 3.1 in 2011, whereas the slope of the GR relationship is marked by a rather uniform b -value ≈ 1 except for the last 2 datapoints.

Summarizing the effects of pressure drop takes time to result in seismicity, and once it does start, the seismic energy released appears to be increasing at a growing rate which is non-linear.

An elaborate statistical analysis on induced seismicity in the Netherlands was conducted in an attempt to identify controlling parameters and provide a framework for a priori hazard estimation (Van Eijs et al., 2006). This study had been based on seismicity data collected until 2004. At the time, of the 124 fields 16 were known to have induced seismicity. Van Eijs et al. (2006) showed that the pressure drop in the reservoir (DP), the ratio of Young's moduli from the overburden and the reservoir (Er) as well as fault

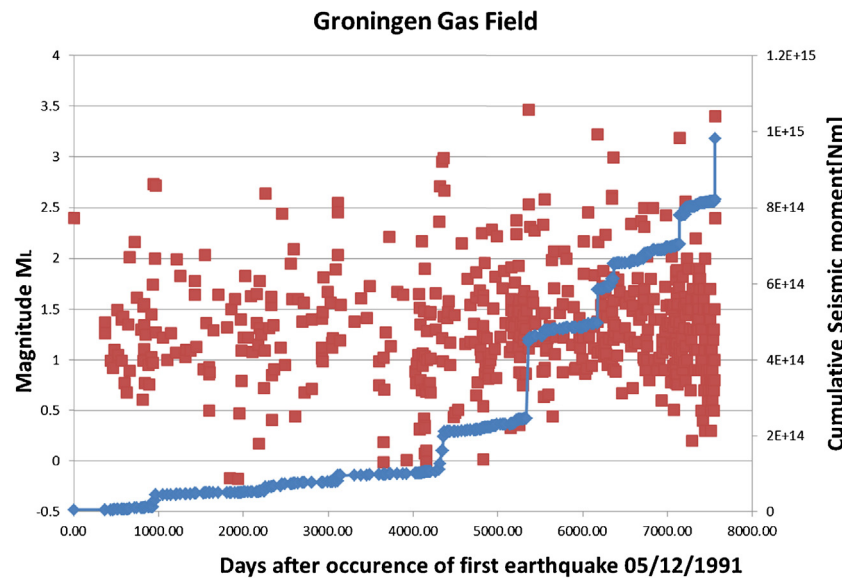


Fig. 4. Local magnitude M_L of induced events in the Groningen Gas Field registered from 5/12/1991 to 16/08/2012, and the cumulative seismic moment in Nm.

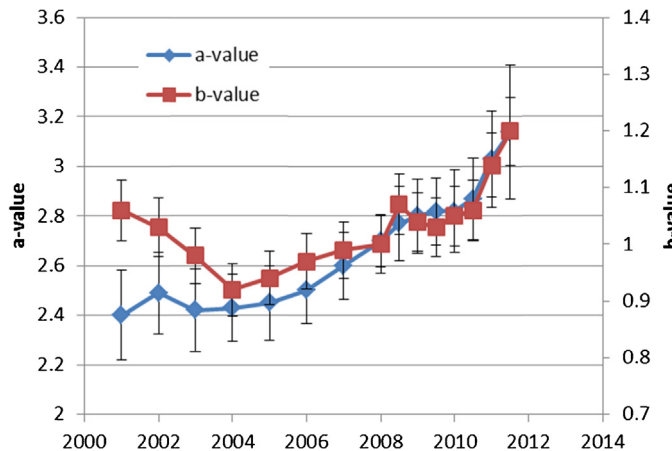


Fig. 5. a and b -values of the Gutenberg–Richter relationship for the seismicity in the Groningen Gas Field. The a and b values have been determined using a sliding time-window of 3 to 5 years, to ensure sufficient events (>50) in each data bin.

density in the reservoir, defined as $F = \text{fault area}^{3/2}/\text{volume}$, are key parameters which can be used to predict the probability of seismicity (Table 1). They drew the following two main conclusions on these parameters:

- From the statistical analysis it appeared that a minimum pressure drop (DP) of 72 bar is required for seismicity to occur. If $Er < 0.93$ no seismicity occurs.

Table 1

Calculation of the probability for induced events for all hydrocarbon fields investigated: situation 2004 (Eijs and Orlic, 2006; Van Eijs et al., 2006) and situation 2010 (Van Thienen-Visser et al., 2012).

2004	Fields marked by seismic events (16)	
	DP > 72 bar	$F > 0.98$ and $Er > 1.34$: $P = 0.52 \pm 0.09$ (12)
	(81)	$F > 0.98$ and $0.93 < Er < 1.34$: $P = 0.10 \pm 0.05$ (36)
	DP < 72 bar (27)	$F < 0.98$ or $Er < 0.93$: $P = 0$ (33)
		$P = 0$ (27)
2010	Fields marked by seismic events (23)	
	DP/ $P_{ini} > 28\%$	$F > 0.86$ and $Er > 1.34$: $P = 0.42 \pm 0.08$ (61)
	(84)	$F > 0.86$ and $1.01 < Er < 1.34$: $P = 0.19 \pm 0.05$ (7)
	DP/ $P_{ini} < 28\%$ (19)	$F < 0.86$ or $Er < 1.01$: $P = 0$ (16)
		$P = 0$ (19)

- The data support that if the fault density $F < 0.98$ then no seismicity would occur. Fault length corresponds to the faults which can be mapped from reservoir structure (e.g. are marked by reservoir offset of 10 m or more) and volume corresponds to the surface area of the reservoir at the gas water contact (GWC) multiplied by the average height.

An update of the analysis has been recently made based on seismicity and production data until May 2010 (Van Thienen-Visser et al., 2012) which allowed to validate and refine the results of (Van Eijs et al., 2006). In 2010, the number of producing fields increased from 124 to 126, and the number of seismically active fields increased from 16 to 23. The number of registered induced events doubled to 800. None of the reservoirs which had been attributed a zero probability for induced events in 2004 have showed seismicity afterwards. The larger number of data also allowed to refine the threshold values proposed in 2006 (Table 1 and Fig. 6). In this refinement, Van Thienen-Visser et al. (2012) proposed to change the pressure drop parameter into a new parameter (DP/P_{ini}) expressing relative depletion as the ratio of pressure drop and initial pressure. To illustrate the influence of fault density, we show in Fig. 7 an overlay of fault structures and seismicity. As the induced seismicity has spatial resolution of about 0.5 km it is not well possible to locate events to individual faults. The map in Fig. 7 shows that the Friesland Platform, which is lacking induced seismicity, has a markedly different structural grain and fault density signature compared to the Groningen High.

4. Proposed mechanism for the induced events: the critical role of faults and in situ stress

The pressure change affects the in-situ stress through poro-elastic coupling. Geomechanical models, demonstrate that the reservoir may compact, resulting in land subsidence (e.g. Geertsma, 1973; Fokker and Orlic, 2006), and at reservoir levels stress concentrations can occur which may result in reactivation of faults (e.g. Segall and Fitzgerald, 1998). In this section we aim to relate – through geomechanical analysis – the level of initial stress, fault orientation, reservoir parameters and depletion characteristics to probability and subsequent evolution of fault reactivation, causing seismicity. Further, we wish to understand their intimate relationship and to relate these to the key observations from the statistical

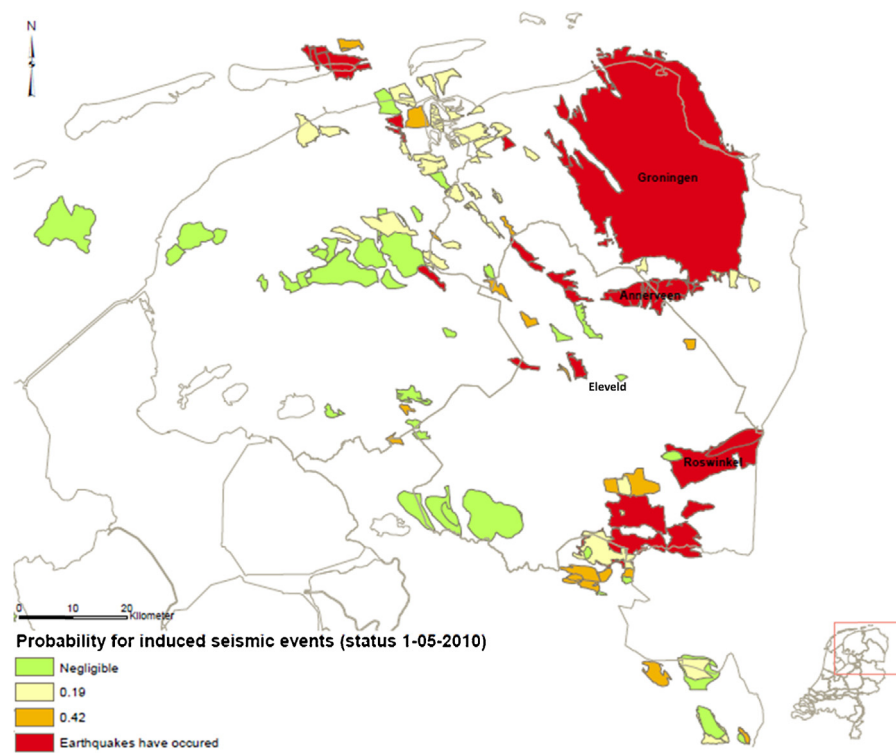


Fig. 6. Probability of induced seismic events for different fields based on the classification in Table 2 for situation 2010 (Van Thienen-Visser et al., 2012).

analysis in the previous section. To that end, we review and present earlier model approaches to numerically assess the effects of initial stress and stress changes related to pressure depletion for laterally extensive and fault bounded reservoirs in Sections 4.1 and 4.2, respectively, and we relate the findings of elastic models to the characteristics of the observed induced seismicity in the Dutch gas fields. In Section 4.3 we present an elasto-plastic geomechanical model, demonstrating that such models can be successfully used

to predict the observed delay in onset of seismicity and increasing growth rate of the cumulative seismic moment (cf. Fig. 4).

4.1. Laterally extensive reservoirs

The first set of models considers reservoirs that are not fault-bounded and laterally extensive. They are considered representative for reservoirs with very low fault density (Fig. 7), which

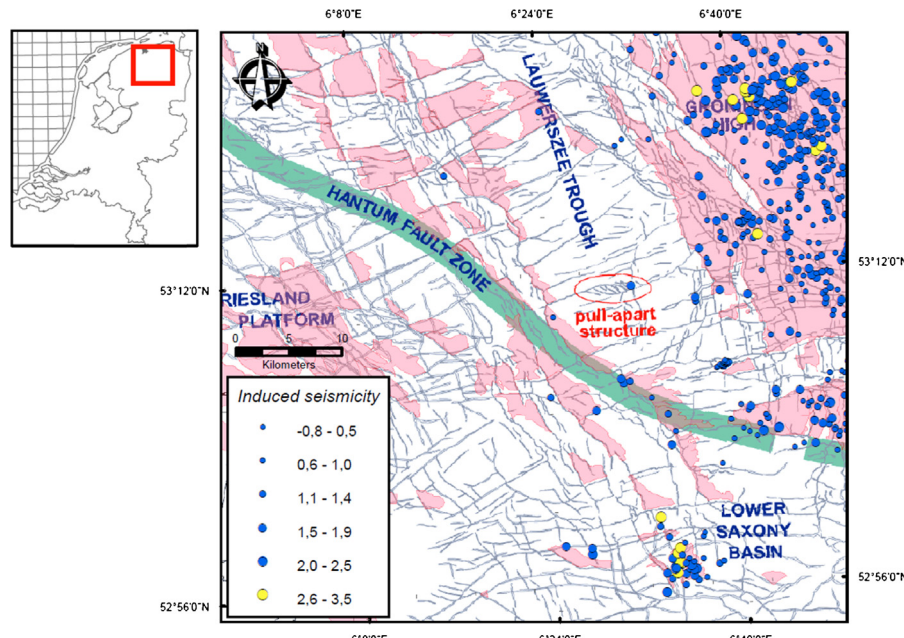


Fig. 7. Fault fabric at Rotliegend reservoir level from high quality 3D seismic interpretation (from De Jager, 2007). The outline of the gas fields is shown, as well as the induced events. Largest events are shown in yellow. (For interpretation of the references to color in this figure legend, the reader is referred to the web version of the article.)
Source: KNMI (2012).

occur for instance in the Friesland Platform. According to the statistical analysis by Van Eijs et al. (2006) and (Van Thienen-Visser et al., 2012) these have negligible probability of seismicity (Fig. 6). Our analysis should thus confirm that for any value of ($\Delta P/P_{ini}$) these type of fields do not produce stress changes which can lead to failure of faults.

In models for reservoir compaction and overpressure generation in basins (Engelder and Fischer, 1994; Hettema et al., 2000; Hillis, 2001; Altmann et al., 2010), it has been noted that stress changes in a center of a laterally infinite compacting reservoir can be expressed through as “pore pressure/stress coupling”. This is based on the poro-elastic response under uniaxial compaction conditions with (a) a horizontal infinitely large reservoir, (b) lateral constant vertical stress, which is given by the overburden's weight and which does neither change laterally nor with changing pore pressure, (c) horizontal strains equal to zero and (d) equal changes in the maximum and the minimum horizontal stresses:¹

$$\frac{\Delta\sigma_h}{\Delta p} = \alpha\gamma_h = \alpha \left(\frac{1-2\nu}{1-\nu} \right) \quad (4)$$

where α is Biot's coefficient. $\alpha\gamma_h$ denotes the pore pressure stress coupling (e.g. Altmann et al., 2010, their PSM), γ_h the stress path parameter normalized to α (cf. Hettema et al., 2000; Soltanzadeh and Hawkes, 2008). The effective stress change becomes:

$$\frac{\Delta\sigma'_h}{\Delta p} = \alpha(\gamma_h - 1) \quad (5a)$$

$$\frac{\Delta\sigma'_v}{\Delta p} = -\alpha \quad (5b)$$

From Eqs. (5a), (5b) and (4), it is obvious that Biot's coefficient scales the stress coupling, whereas ν influences the ratio of horizontal and vertical stress change. Measured values for $\alpha\gamma_h$ vary considerably in line with possible variation in α , ν and deviation from the simplified boundary conditions of uniaxial compaction (Altmann et al., 2010).

The effective stress ratio as a function of pressure change, initial stress ratio $K'_{initial}$ and lithostatic and hydrostatic gradient becomes:

$$K'(\Delta p) = \frac{\sigma'_h}{\sigma'_v} = \left(\frac{K'_{initial}(\rho_l - \rho_w) + \alpha(\gamma_h - 1)q}{(\rho_l - \rho_w) - \alpha q} \right) \quad (6)$$

where ρ_l is the bulk density in agreement with the lithostatic gradient; ρ_w the apparent water density which reflects the pressure gradient, and the parameter $q = (\Delta p/P_{ini})\rho_w$, which is negative for depletion. The relation demonstrates that the effective stress ratio response is insensitive to the actual depth of the reservoir.

Fig. 8 illustrates the change in effective stress ratio K' as a function of reservoir depletion, adopting parameters which are representative for Dutch reservoirs. $\rho_l = 2.2 \text{ g/cm}^3$, $\rho_w = 1 \text{ g/cm}^3$. α has been estimated close to 1, as it is marked by high porosities. Poisson's ratio, which has been determined for Dutch reservoir rocks in the range of 0.15–0.3 (e.g. Mulders, 2003). In the reservoir, stress conditions on faults which are favorably oriented to the stress field get more proximal to failure depending on the Poisson's ratio in conjunction with the coefficient of friction of faults. For reference we adopt a coefficient of friction of 0.6, which corresponds to a critical effective stress ratio $K'_\mu = 0.32$. It is evident that stress effects are moderate and do not lead to failure, except for values of $K'_{initial}$ which are moderately above K'_μ . For a higher coefficient of friction, $K'_{initial}$ and K'_μ would shift to higher values. Fig. 9 shows the effect for progressive depletion in a Mohr–Coulomb diagram as stress paths

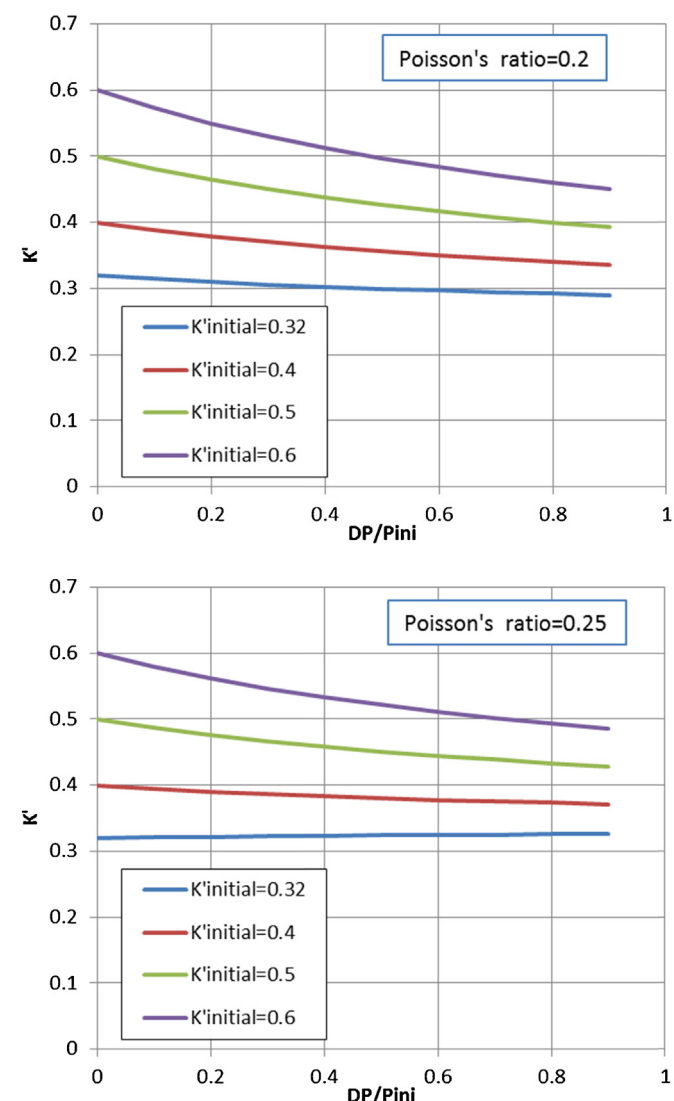


Fig. 8. Change of effective stress ratio (K') for gas depletion in the center of a laterally extensive reservoir as a function of different $K'_{initial}$ values. (top) $\nu=0.2$, (bottom) $\nu=0.25$, based on Eqs. (5a) and (5b) in text.

for faults which are favorably oriented in the stress field, highlighting that considerable stress changes do hardly result in moving the Mohr circle closer to the failure envelope.

In an analysis of gas depletion in Northeast Netherlands, Van Wees et al. (2003) concluded that for non-critical stress conditions

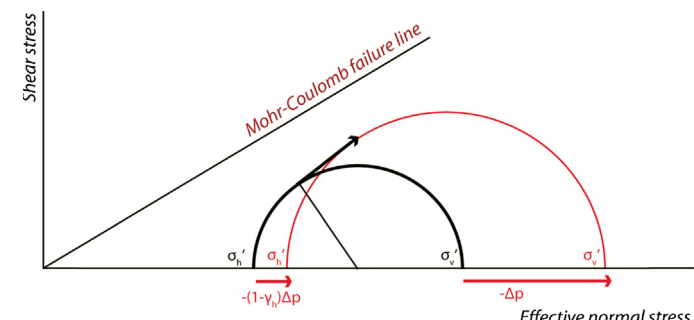


Fig. 9. Changes in effective stress for gas depletion in a laterally extensive aquifer and its effect of stabilizing or destabilizing stress for slip on faults inside the reservoir for $K'_{initial} = 0.5$ and a pressure drop ($\Delta P/P_{ini}$) of 40%, based on Eqs. (5a) and (5b) in text. Adopted coefficient of friction μ and Poisson's ratio $\nu=0.2$.

¹ Compressive stresses are denoted positive as well as pressure. A negative pressure change Δp corresponds to depletion, so $\Delta p = -DP$.

in agreement with $K'_{\text{initial}} = 0.5$, failure on pre-existing faults in laterally extensive reservoirs would indeed require very low friction coefficients (<0.3) for the faults. For a friction coefficient of 0.6 and non-critical initial stress state such as inferred for the northern Netherlands, it appears not possible for laterally extensive fields to generate induced seismicity.

Altmann et al. (2010) noted that the stress path parameters can vary laterally because of lateral pressure differences during depletion, and that these could alter significantly the stress effects, for laterally extensive reservoir geometries. However, most Dutch gas fields are likely marked by sufficiently high permeability to prevent significant pressure differences. For the very large Groningen Gas Field lateral pressure difference are limited to ca. 5% of the initial pressure (NAM, 2010).

4.2. Differential compaction for faulted reservoirs

In the past decade many analytical and numerical geomechanical studies have focused on the stress effects in and outside the reservoir related to specific reservoir geometries. From analytical approaches it has become clear that effective stress changes, due to differential compaction, are not in agreement with uniaxial assumptions proposed in the previous paragraph, especially close to the edges of the reservoir (e.g. Segall and Fitzgerald, 1998; Hillis, 2001; Khan & Teufel, 2000; Soltanzadeh and Hawkes, 2008). The semi-analytical analysis of Soltanzadeh and Hawkes (2008) for reservoirs with rectangular cross section geometry (x, y direction) with plane strain conditions (z -direction) is very instructive for the spatial characteristics of destabilization of stresses inside and outside the reservoir in relation to a fault bounded reservoir geometry. They propose a more generalized form of Eq. (4) to define stress path parameters for the different components of the stress tensor:

$$\text{Inside the reservoir : } \frac{\Delta \sigma'_{ij}}{\Delta p} = \alpha(\gamma_{\alpha(ij)} - \delta_{ij}) \quad (7a)$$

$$\text{Outside the reservoir : } \frac{\Delta \sigma'_{ij}}{\Delta p} = \alpha \gamma_{\alpha(ij)} \quad (7b)$$

Here $\gamma_{\alpha(ij)}$ corresponds to normalized stress path parameters which vary in space and can be determined from the analytical or numerical model results. The largest variation of stress path parameters and associated destabilization of stress take place along the horizontal center-line of the reservoir. Here $\gamma_{\alpha(12)} = 0$. Fig. 10 illustrates the cross sectional horizontal stress parameter $\gamma_{\alpha(11)}$ and vertical stress parameter $\gamma_{\alpha(22)}$ along this line. $\gamma_{\alpha(11)}$ reaches a maximum close to $\gamma_h = ((1-2\nu)/(1-\nu))$ near the center of the reservoir, in agreement with the uniaxial solution of Eqs. (5a) and (5b). Toward the edge of the reservoir it decreases quickly, reaching about $\gamma_{h/2}$ on the edge, whereas outside the reservoir it decreases to 0. The vertical stress parameter $\gamma_{\alpha(22)}$ is close to zero in the center of the reservoir and reaches its maximum at the edge of the reservoir, reaching a value of about $\gamma_{h/2}$. Over the edge there is a lateral discontinuity of the vertical stress path parameter, as a consequence of required continuity in the total stress (Soltanzadeh and Hawkes, 2008):

$$\gamma_{\alpha(22)}^{\text{INSIDE}} - \gamma_{\alpha(22)}^{\text{OUTSIDE}} = \gamma_h \quad (8)$$

where $\gamma_{\alpha(22)}^{\text{OUTSIDE}}$ is equal to $-\gamma_{h/2}$. Therefore, the horizontal and vertical stress path parameter just outside of the edge of the reservoir result in strongest destabilization of the effective stress ratio for gas depletion:

$$K'(\Delta p)^{\text{OUTSIDE}} = \left(\frac{K'_{\text{initial}}(\rho_l - \rho_w) + \alpha(\gamma_h/2)q}{(\rho_l - \rho_w) - \alpha(\gamma_h/2)q} \right) \quad (9)$$

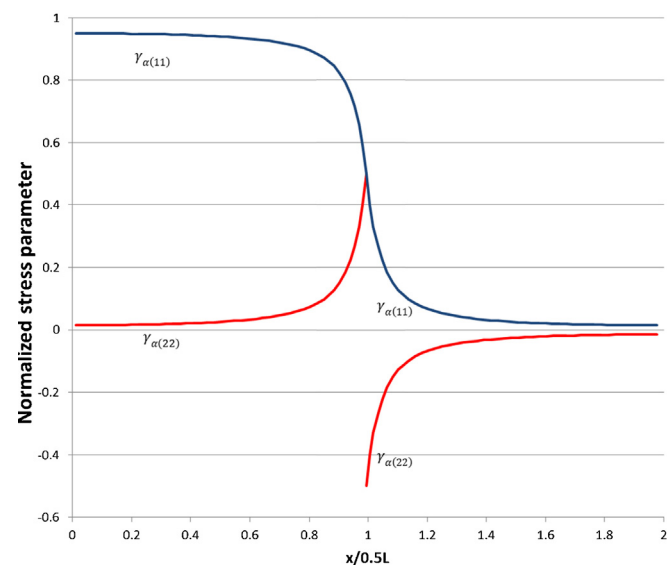


Fig. 10. Schematic stress path parameters $\gamma_{\alpha(11)}$ and $\gamma_{\alpha(22)}$ of horizontal and vertical stress respectively long a horizontal mid-line of a reservoir with rectangular geometry under plane strain conditions (after). X coordinate is scaled to the half length of the reservoir. The ratio of half length and height is 10. Length and depth are equal.

As q is negative with pressure depletion, the stress ratio is rapidly decreasing with progressive depletion. In Fig. 11, we have used Eq. (8) to plot for a range of initial stress ratios the change in K' . From these curves it is evident that for all initial stress conditions a significant drop in K' occurs with depletion. Fig. 12 shows this effect for progressive depletion in a Mohr–Coulomb diagram as stress paths for faults which are favorably oriented in the stress field, highlighting that considerable stress changes move the Mohr circle closer to the failure envelope.

For a critically stressed reservoir ($K'_{\text{initial}} = 0.32$), favorably oriented faults would slip almost immediately at the initial stage of depletion. For more stable initial stress conditions, the reservoir faults will not immediately start to fail but after some period of depletion, which can be equivalent to reducing initial reservoir pressure by as much as 25% to 80%, for $K'_{\text{initial}} = 0.4$ and $K'_{\text{initial}} = 0.6$, respectively.

Many Dutch gas reservoirs are fault bounded or internally offset by faults. Examples are the Annerveen, Eleveld, Groningen, and Roswinkel fields (Fig. 6). Consequently, differential compaction due to faults bounding or intersecting and displacing the reservoir top or Gas water contact, plays a dominant role in generating critical stress on faults. From the regional stress field interpretation in Section 2, we infer that NW–SE oriented normal faults in reservoirs align to the S_H orientation, and dips can be such that they may be favorably oriented for failure. An example of a field with many of such faults is the Groningen Gas Field (Fig. 7). For fields in other settings, such as the Annerveen field, reactivation of differentially oriented faults can possibly be explained by a ratio close to 1 of σ_H and σ_v , or σ_h and σ_H .

To date, for Dutch reservoirs a few geomechanical numerical modeling studies have studied in situ stress changes and fault reactivation potential associated with gas extraction. Two-dimensional numerical studies have been published on the Eleveld gas field (Roest and Kuilman, 1994) and a produced field used for underground gas storage (UGS) (Nagelhout and Roest, 1997). Mulders (2003) and Orlic and Wassing (2012) analyzed with finite element models the stress parameters for a radial symmetric fault-bounded disk-shaped reservoir adopting reservoir geometries representative for Dutch gas depletion, and tested the sensitivity to variability in various rock parameters. Reported K'_{initial} in

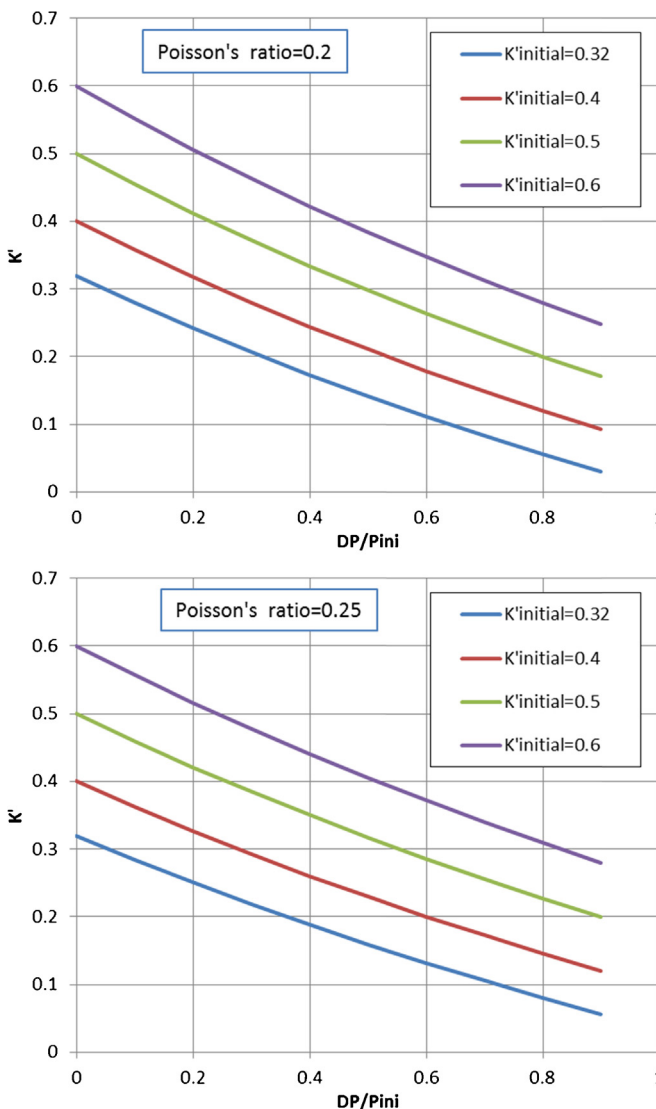


Fig. 11. Change of effective stress ratio (K') for gas depletion at the fault just outside the edge of reservoir as a function of different K'_{initial} values. (top) $v=0.2$, (bottom) $v=0.25$, based on Eq. (8) in text.

geomechanical models are typically marked by a $K'_{\text{initial}} = 0.5$ (e.g. Orlic and Wassing, 2012).

These models reproduce successfully the destabilization of faults and the time delay in onset of seismicity. However, apart from Poisson's ratio the following effects need to be taken into account for fault bounded reservoirs:

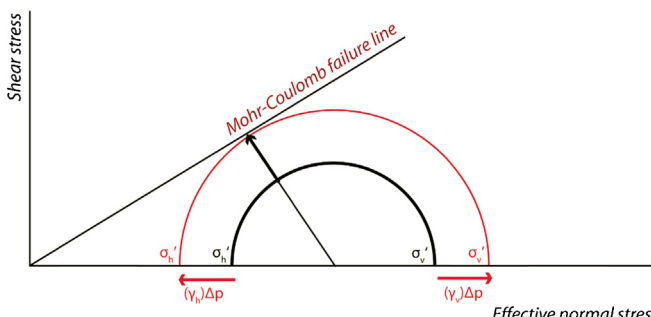


Fig. 12. Changes in effective stress for slip on a fault just outside the reservoir for $K'=0.5$ and a pressure drop (DP/P_{ini}) of 33%. Adopted coefficient of friction μ and Poisson's ratio $v=0.2$.

- The ratio of height and width of the reservoir has a strong effect on the spatial characteristics of $\gamma_{\alpha(ij)}$. For geometries which are representative for Dutch gas fields marked by a typical thickness to half-length ratios of about 10, and depth to thickness ratio's exceeding 10 (Mulders, 2003; Orlic and Wassing, 2012), the magnitude of the stress path parameters is hardly changing at the side bounding faults/edge on the horizontal mid-line, if these ratios are changed (Soltanzadeh and Hawkes, 2008).
- The characteristics of $\gamma_{\alpha(ij)}$ at the horizontal mid-line of the reservoir are not much variable for changing vertical faults to more realistic steeply dipping faults at the side boundary (e.g. Mulders, 2003).
- The thickness of the reservoir at the side boundary, plays an important factor in the areal extent at the side which is marked by exceedence of critical stress (e.g. Orlic and Wassing, 2012). Since the seismic moment of an event is proportional to the slipping area of the fault, the thickness is expected to play an important role in the level of seismicity which can be generated, through an increase of the area of seismic slip and the associated displacement.
- A contrast in the ratio of Young's moduli of overburden and reservoir (parameter E_r in the statistical analysis of the Section 3) has a significant effect on the maximum values of $\gamma_{\alpha(ij)}$ which can be attained. For a ratio of 0.7, the values can drop by more than 50% (Mulders, 2003). As a result, K' decreases at less steep gradient with depletion, and the faults may not become critically stressed.
- The reduction of K' can be enhanced by combined contributions of differential compaction of adjacent reservoir compartments vertically offset by a fault (e.g. Mulders, 2003; Orlic and Wassing, 2012)
- Creep effects in evaporite cap rocks can result in time dependent effects (e.g. Orlic and Wassing, 2012).

4.3. Seismic moment and magnitude prediction

In the previous section we reviewed elastic stress effects for differential compaction, capable of generating fault rupture. Geomechanical models, incorporating frictional sliding, can be used to predict deterministically the evolution over time of fault rupture and relate this to the evolution of cumulative seismic moment CSM:

$$\text{CSM} = \int G u dA \quad (10)$$

where G is shear modulus, u is fault displacement and A is fault area. From the CSM a maximum magnitude can be determined, substituting CSM for M_0 in Eq. (2). This we consider to be a conservative estimate for the maximum possible magnitude since it is assumed that CSM is released in a single seismic event.

A more realistic approach is to assume CSM to be released in N events based on a GR relationship with a constant b -value, and which is truncated at a maximum magnitude. The Moment M_{0x} for event number x and the ratio of cumulative seismic moment of the CSM and $M_{0\text{max}}$:

$$M_{0x} = M_{0\text{max}} x^c \quad (11a)$$

$$\frac{\text{CSM}}{M_{0\text{max}}} = \int_{0.6}^{\infty} x^c dx = \left[\frac{1}{1+c} x^{c+1} \right]_{0.6}^{\infty} \approx -\frac{1}{1+c} 0.6^{c+1} \quad (11b)$$

where $M_{0\text{max}} = 10^{((a/b)+6.07)1.5}$ is the moment of the largest event ($x=1$), $c=-1.5/b$. The lower bound of the integral is based on numerical inspection of the equivalence of the integral of Eq. (11b) for the interval $[x-0.4, x+0.6]$ with the moment from Eq. (11a) corrected for $M_{0\text{max}}$. Eq. (11b) yields a simple relationship for the ratio of the seismic moment of the largest event with probability 1 to occur and the cumulative seismic moment, as a function of

Table 2

Model parameters for 3D elasto-plastic model, of which results are presented in Figs. 14 and 15.

Parameter	Value	Description
l	1000 [m]	Side length of the square reservoir (in map view)
H	150 [m]	Height of the reservoir
Depth	2800[m]	Gas water contact
μ	0.6 [–]	Coefficient of friction
δ	60°	Fault dip
E	18 [GPa]	Young's modulus
v	0.18 [–]	Poisson's ratio
E_r	1 [–]	Ratio of Young's moduli of overburden and reservoir rock
P_{ini}	280 [bar]	Initial reservoir pressure

b -value only. For b -values of 1 and 1.2, 38%, respectively 20% of CSM would be released in the largest event. This corresponds to a correction of maximum expected magnitudes using CSM in Eq. (1), by -0.27 and -0.43 , respectively.

A capability of geomechanical models for predicting the evolution of CSM and maximum magnitudes requires that it not only explains the delay in the onset of seismicity but also the non-linear characteristics of CSM such as observed in the Groningen Gas Field (Fig. 4) and linear trends in the increase of magnitudes (Fig. 3).

We used a 3D geomechanical model of differential compaction for a simplified reservoir and fault geometry (Fig. 13). The model parameters are listed in Table 2. The reservoir has a square shape in map view with side length of 1000 m, and a thickness of 150 m. On one of the 4 sides the reservoir is bounded by a fault dipping away at dip δ from the reservoir. The strike of the side and fault align. In strike direction, the fault measures 2000 m, extending 500 m beyond the side boundary of the reservoir. In dip direction the fault is 1000 m, starting at the top of the reservoir. This agrees with observed upwards truncation of the faults by a thick salt layer acting as cap rock. The reservoir geometry is not representative for the full complexity of Groningen Gas Field dimensions of 10s of km and 100s of intersecting faults (e.g. Fig. 7), but detailed structural information on the reservoir geometry and faults are not available in the public domain, and the simplified model captures conceptually well the effects of differential compaction (cf. Orlic and Wassing, 2012). Mechanical properties for the reservoir have been adopted from

Orlic and Wassing (2012). The initial in situ stress is marked by largest principal stress being vertical σ_v based on an overburden weight adopting a bulk rock density of 2.2 g/cm³. σ_h is aligned in the strike of the fault with an initial value set by the stress ratio $\sigma_h/\sigma_v = 0.9$. Similarly the initial value of σ_h is set by a stress ratio σ_h/σ_v . For the evaluation of effective stresses on the fault zone (just outside the reservoir) hydrostatic pressures have been assumed based on an average water density of 1 g/cm³. We adopted a coefficient of friction of 0.6 for the fault, and have chosen the dip of the fault dip $\delta = 60^\circ$ to be optimal oriented for failure in the tectonic stress regime.

The initial pressure in the reservoir has been chosen at 280 bars. The stress effects of pressure depletion and rupture have been calculated in 5000 load steps adopting analytical point sources for compaction (cf. Geertsma, 1973; Fokker and Orlic, 2006) spaced at 150 m distance, far away from the faults, to 2.5 m spacing close to the fault. The fault itself is represented by square sources (cf. Okada, 1992), with 25 m side length. After each load step, the stresses on the fault patches are evaluated and if these exceed the Mohr Coulomb failure criterion, they will slip through an iterative procedure such that the stresses become in equilibrium with the failure criterion (cf. Zielke and Arrowsmith, 2008).

Fig. 14 shows the results of the model in terms of predicted evolution of Cumulative seismic moment CSM, normalized to its end value and the maximum expected magnitudes cf. Eqs. (11a) and (11b), adopting a b -value of 1. The results are shown as a function of the ratio of pressure drop DP and initial pressure P_{ini} . Fig. 14 demonstrates a strong sensitivity to the chosen initial stress ratios. When the value is close to critically stressing the fault ($K'_{initial} = 0.34$, $\sigma_h/\sigma_v = 0.64$), rupture occurs at a relatively early stage, whereas for more stable initial stress conditions ($K'_{initial} = 0.43$, $\sigma_h/\sigma_v = 0.69$), and ($K'_{initial} = 0.50$, $\sigma_h/\sigma_v = 0.73$), rupture is delayed, in agreement with the conclusions from Section 4.2. The onset of seismicity is predicted slightly later than expected from the analytical solution for the horizontal mid-line of the reservoir with $v = 0.2$ (Fig. 11). This is explained by the fact that the horizontal mid-line is marked by most pronounced stress effects diminishing up-dip and down-dip on the fault, which in stress integration of the patches result in slightly lower stress effects, and slight differences in stress effects from the plane strain formulation and the 3D model. The predicted evolution of normalized CSM, and the maximum magnitude expected is strongly dependent on the initial state of stress. If the faults are initially relatively critically stressed ($K'_{initial} = 0.34$) the CSM increases at an almost linear rate, resulting in a rapid initial growth of maximum magnitudes with slower increase in later stages of depletion. For a less critically stressed fault ($K'_{initial} = 0.50$), the CSM shows a more convex increase and a more linear increase in magnitudes. The latter is more in line with the observations for cumulative seismic moment evolution and magnitudes (Figs. 3 and 4). The non-linear growth in CSM occurs because of the growth of the rupture area, which declines over time.

We investigated the sensitivity of the prediction for a fault orientation deviating from an optimal orientation in the tectonic stress field, as it is likely that pre-existing fault transecting and bounding the reservoir are not optimally oriented (cf. Fig. 7). To this end, we have rerun the models for a horizontal deviation of 20° of the strike of the fault to σ_H . The results in Fig. 15 show a slightly longer delay and slower growth of magnitudes, and smaller maximum magnitudes compared to the optimal oriented fault. This suggests that suboptimal orientation of the pre-existing faults involved in differential compaction can explain the delay in seismicity and non-linear growth rate. However, it should be noted that if deviation from optimal orientation would be too large and initial stress would be relatively close to critical, new rupture surfaces could be formed early on, as K' drops below the critical value of $K'_\mu = 0.32$ for a coefficient of friction $\mu = 0.6$ (cf. Fig. 11).

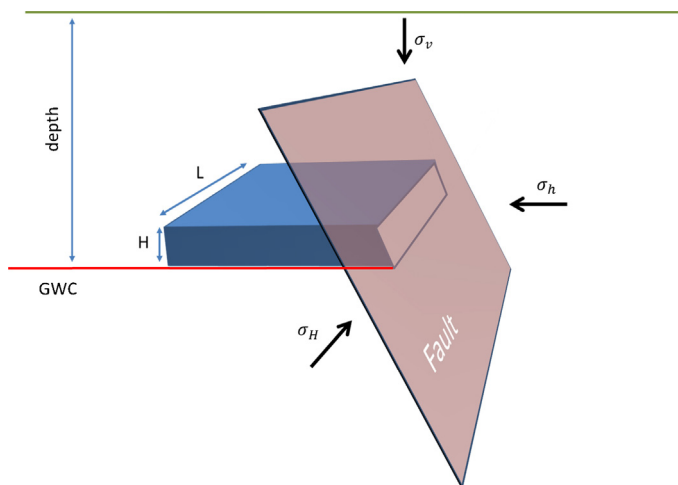
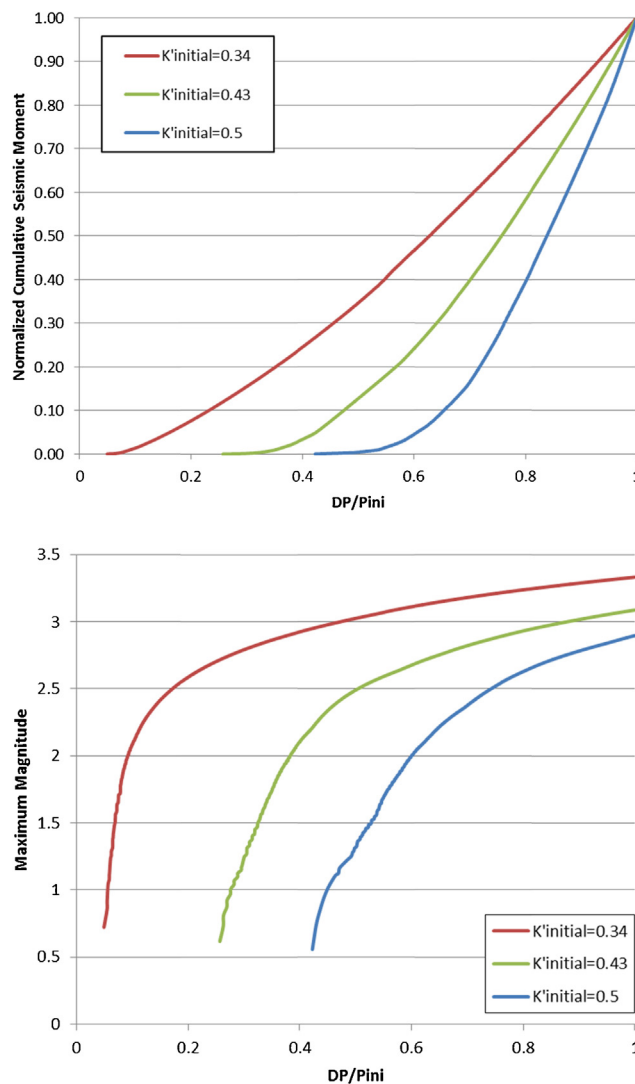


Fig. 13. Schematic cartoon of the geomechanical model for compaction, with compacting gas reservoir with side length L and thickness H bounded at one side by a fault, favorably aligned for slip in the stress field at dip $\delta = 60^\circ$. GWC denotes gas water contact. See text and Table 2 for details.



Summarizing, the numerical models contend that the initial stress ratio is most likely not close to the critical stress values for failure of existing faults. Most importantly, in none of the depleted gas fields seismicity has been observed prior to a drop of 28% in reservoir pressure (Fig. 3). A critical stress state would trigger seismic events from the start, if the faults are close to optimally oriented. The observed convex evolution of normalized CSM in the Groningen Gas Field (Fig. 4) and the rather linear increase in maximum magnitude (Figs. 3 and 5) appears to be consistent with a model in which faults are not critically stressed at the onset of depletion. This effect relates to different growth characteristics of the rupture area for critically stressed versus non-critically stressed faults.

The presented semi-generic model serves to highlight key aspects of the interaction of initial stress and differential compaction in the framework of induced seismicity in Dutch gas fields. It is not intended as predictive model for induced seismicity in a particular field. To this end, a much more detailed field specific study, taking into account the full complexity of reservoir geometry, depletion history, and mechanical properties is required.

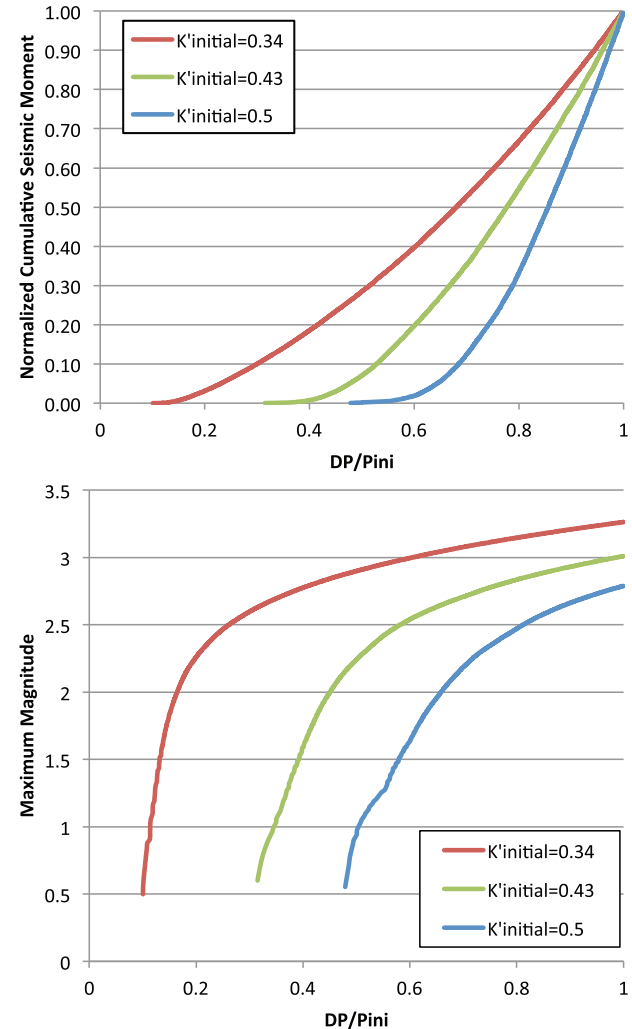


Fig. 15. Results from the geomechanical model with horizontal deviation of 20° of the strike of the fault to σ_H^o . (A) Evolution of cumulative seismic moment (CSM), normalized to its end value and (B) maximum magnitude from CSM (Eqs. (11a) and (11b)) from frictional sliding in the model adopting a b -value of 1. See text and Table 2 for details.

5. Conclusions

In this paper we presented a review of controlling geological, tectonic and engineering factors for induced seismicity associated to gas depletion in the Netherlands, where 190 gas fields of varying size have been exploited. No more than 15% of these fields show seismicity, which is being closely monitored. Geomechanical studies indicate that largest seismicity is localized on pre-existing fault structures. The prime cause for seismicity in gas depletion is differential compaction. Stress measurements from leak-off pressure and the accumulated pressure development prior to induced seismic events show that most faults are generally far from critically stressed prior to gas depletion. We used geomechanical models to show that non-critical stresses on faults can well explain the delay of seismic events to occur not prior to 28% of depletion, and that a non-critical initial stress state is in agreement with the observed trend of rather linear increase of maximum magnitude and convex increase of cumulative seismic moment. The presented model serves to highlight key aspects of the interaction of initial stress and differential compaction in the framework of induced seismicity in Dutch gas fields. It is not intended as predictive model for induced seismicity in a particular field. To this end, a much more detailed field specific study, taking into account the full complexity

of reservoir geometry, depletion history, and mechanical properties is required.

Our study highlights the importance of taking into account the criticality of stress on faults – as a function of in-situ stress, fault geometry and frictional properties – to assess expected maximum magnitude, as a consequence of differential compaction. Differential compaction is theoretically expected to occur as well in geothermal systems, in particular in reservoirs where the fluid volumes extracted are significantly larger than the re-injected volumes, and which have resulted in reservoir compaction, supported by land subsidence observations such as the Geysers (eg. Mossop and Segall, 1997). Consequently, if one would like to assess a priori the amount and in particular the maximum magnitude of induced events in such reservoirs, knowledge of the (initial) in situ stress, pore pressure, fault pattern (length of segments) and properties are needed. For the stimulation phase of EGS systems, the mechanism of generating induced events is primarily related to fluid pressure diffusion (e.g. Baisch et al., 2010). However the a priori assessment of the in situ stress, fault geometry and properties would be equally important.

Acknowledgements

This paper benefited from constructive comments from Oliver Heidbach and an anonymous reviewer. This work was funded by the GEISER European Project (FP7:241321).

References

- Aki, K., 1966. Generation and propagation of G waves from the Niigata earthquake of June 16, 1964. Part 2. Estimation of earthquake moment, released energy, and stress-strain drop from the G wave spectrum. *Bull. Earthquake Res. Inst.* 44, 73–88.
- Altmann, J.B., Heidbach, O., Gritto, R., 2013. Relative importance of processes leading to stress changes in the Geysers geothermal area. In: Proceedings, Thirty-Eighth Workshop on Geothermal Reservoir Engineering, February 11–13, Stanford University, Stanford, CA, SGP-TR-198.
- Altmann, J.B., Müller, T.M., Müller, B.I.R., Tingay, M.R.P., Heidbach, O., 2010. Poroelastic contribution to the reservoir stress path. *Int. J. Rock Mech. Mining Sci.* 47 (7), 1104–1113.
- Baisch, S., Vörös, R., Rothert, E., Stang, H., Jung, R., Schellschmidt, R., 2010. A numerical model for fluid injection induced seismicity at Soultz-sous-Forêts. *Int. J. Rock Mech. Mining Sci.* 47, 405.
- Breckels, I.M., Van Eckelen, H.A.M., 1982. Relationship between horizontal stress and depth in sedimentary basins. Society of Petroleum Engineers, SPE10336.
- Byerlee, J., 1978. Friction of rocks. *Pure Appl. Geophys.* 116 (4), 615–626.
- Camelbeeck, T., 1994. The 1992 Roermond earthquake, the Netherlands, and its aftershocks. *Geol. En Mijnbouw* 73 (2–4), 181–197.
- Camelbeeck, T., Van Eck, T., 1994. The Roer Valley Graben earthquake of 13 April 1992 and its seismotectonic setting. *Terra Nova* 6 (3), 291–300.
- Cloetingh, S., van Wees, J.D., Ziegler, P.A., Lenkey, L., Beekman, F., Tesauro, M., Worum, G., 2010. Lithosphere tectonics and thermo-mechanical properties: an integrated modelling approach for Enhanced Geothermal Systems exploration in Europe. *Earth-Sci. Rev.* 102 (3–4), 159–206.
- Dirkzwager, J.B., van Wees, J.D.V., Cloetingh, S.A.P.L., Geluk, M.C., Dost, B., Beekman, F., 2000. Geo-mechanical and rheological modelling of upper crustal faults and their near-surface expression in the Netherlands. *Global Planet. Change* 27, 67.
- Dost, B., Goutbeek, F., Van Eck, T., Kraaijpoel, D., 2012. Monitoring induced seismicity in the North of the Netherlands: status report 2010. Report No. WR 2012-13. Royal Netherlands Meteorological Institute, De Bilt.
- Eck, T.v., Goutbeek, F., Haak, H., Dost, B., 2006. Seismic hazard due to small-magnitude, shallow-source, induced earthquakes in the Netherlands. *Eng. Geol.* 87, 105.
- Eijs, R.M.H.E.V., Orlic, B., 2006. Status report on numerical results of well integrity analysis (No. 2006-U-R0079/B). TNO, Utrecht.
- Engelder, T., Fischer, M.P., 1994. Influence of poroelastic behavior on the magnitude of minimum horizontal stress, sh in overpressured parts of sedimentary basins. *Geology* 22 (October (10)), 949–952.
- Evans, K.F., Zappone, A., Kraft, T., Deichmann, N., Moia, F., 2012. A survey of the induced seismic responses to fluid injection in geothermal and CO₂ reservoirs in Europe. *Geothermics* 41 (0), 30–54.
- Fjaer, E., Holt, R.M., Horsrud, P., Raaben, A.M., Risnes, R., 1993. Petroleum Related Rock Mechanics. Elsevier, Retrieved from: <http://tsn.tno.nl/Data\SV\sv-044425\articles\Books\Fjaer.2008.Petroleum.related.rock.mechanics.pdf>
- Frikken, H.W., 1996. Sub-horizontal drilling: remedy for under-performing Rotliegend gasfields, L13 block, central offshore Netherlands. In: Rondeel, H.E.,
- Batjes, D.A.J., Nieuwenhuijs, W.H. (Eds.), *Geology of Gas and Oil Under the Netherlands.*, 1st ed. Springer, Dordrecht, p. 115.
- Fokker, P.A., Orlic, B., 2006. Semi-analytic modelling of subsidence. *Math. Geol.* 38 (5), 565–589.
- Hanks, T.C., Kanamori, H., 1979. A moment magnitude scale. *J. Geophys. Res.* 84 (85).
- Geertsma, J., 1973. Land subsidence above compacting oil and gas reservoirs. *J. Petrol. Technol. June*, 734.
- Gölke, M., Coblenz, D., 1996. Origins of the European regional stress field. *Tectonophysics* 266 (1–4), 11–24.
- Grünthal, G., Stromeier, D., 1992. The recent crustal stress field in Central Europe: trajectories and finite element modeling. *J. Geophys. Res.* 97 (B8), 11,805.
- Heidbach, O., Tingay, M., Barth, A., Reinecker, J., Kurfeß, D., Müller, B., 2010. Global crustal stress pattern based on the world stress map database release 2008. *Tectonophysics* 482 (1–4), 3–15.
- Hettema, M.H.H., Schutjens, P.M.T.M., Verboom, B.J.M., Gussinklo, H.J., 2000. Production-induced compaction of a sandstone reservoir: the strong influence of stress path. In: SPE Reservoir Evaluation and Engineering, August.
- Hillis, R.R., 2001. Coupled changes in pore pressure and stress in oil fields and sedimentary basins. *Petrol. Geosci.* 7 (4), 419–425.
- Hofstee, C., Benedictus, T., ter Heege, J., Huibregtse, J., van der Meer, B., Nelskamp, S., Orlic, B., Pluymaekers, M., Tambach, T., 2009. Feasibility of CO₂ storage in the Friesland platform. TNO-034-UT-2009-01084.
- Jaeger, J.C., Cook, N.G.W., 1969. *Fundamentals of Rock Mechanics*.
- Khan, M., Teufel, L.W., 2000. The effect of geological and geomechanical parameters on reservoir stress path and its importance in studying permeability anisotropy. *SPE Reserv. Eval. Eng.* 3 (October), 394.
- KNMI (2012). www.knmi.nl, website of Royal Netherlands Meteorological Institute (KNMI) (accessed October 2012).
- Kohl, T., Megel, T., 2007. Predictive modeling of reservoir response to hydraulic stimulations at the European EGS site Soultz-sous-Forêts. *Int. J. Rock Mech. Mining Sci.* 44, 1118.
- Kombrink, H., Doornenbal, J.C., Duin, E.J.T., Den Dulk, M., Van Gessel, S.F., Ten Veen, J.H., Witmans, N., 2012. New Insights into the geological structure of the Netherlands; results of a detailed mapping project. *Neth. J. Geosci.* 91 (4), 419–446.
- McGarr, A., 2002. Case histories of induced and triggered seismicity. In: Lee, W.H.K., Kanamori, H., Jennings, P.C., Kisslinger, C. (Eds.), *International Handbook of Earthquake and Engineering Seismology*, 81A ed. p. 647.
- Moeck, I., Backers, T., 2011. Fault reactivation potential as a critical factor during reservoir stimulation. *First Break*, 29.
- Mossop, A., Segall, P., 1997. Subsidence at The Geysers Geothermal Field, N. California from a comparison of GPS and leveling surveys. *Geophys. Res. Lett.* 24 (14), 1839–1842.
- Mossop, A., Segall, P., 1999. Volume strain within the Geysers geothermal field. *J. Geophys. Res.* 104 (B12), 29,113–29,131.
- Mulders, F.M.M., (Doctoral thesis) 2003. *Modelling of Stress Development and Fault Slip in and Around a Producing Gas Reservoir*. Technical University of Delft, Delft.
- Muntendam-Bos, A.G., De Waal, J.A., 2013. Reassessment of the probability of higher magnitude earthquakes in the Groningen gas field. State Supervision of Mines. <http://www.sodnm.nl/sites/default/files/redactie/20130116%20groningen%20seismicity%20report%20final.pdf>
- Nagelhout, A.C.G., Roest, J.P.A., 1997. Investigating fault slip in a model of an underground gas storage facility. *Int. J. Rock Mech. Mining Sci.* 34 (3–4), 212.e1–212.e14.
- NAM, 2010. Bodemdalting door Aardgaswinning (in dutch). Nederlandse Aardolie Maatschappij document EP201006302236.
- NLOG, 2012. Dutch oil and gas data portal of the Geological Survey of the Netherlands-TNO, <http://nlog.nl> (accessed October 2012).
- Orlic, B., Wassing, B.B.T., 2012. A study of stress change and fault slip in producing gas reservoirs overlain by elastic and visco-elastic caprocks. *Rock Mech. Rock Eng.*, <http://dx.doi.org/10.1007/s00603-012-0347-6>.
- Okada, Y., 1992. Internal deformation due to shear and tensile faults in a half-space. *Bull. Seismol. Soc. Am.* 82 (2), 1018.
- Plenefisch, T., Bonjer, K., 1997. The stress field in the Rhine Graben area inferred from earthquake focal mechanisms and estimation of frictional parameters. *Tectonophysics* 275 (1–3), 71–97.
- Roest, J.P.A., Kuilman, W., 1994. Geomechanical analysis of small earthquakes at the Eleverbeld gas reservoir. *SPE 28097*.
- Rondeel, H.E., Everaars, J.S.L., 1993. Spanning in NoordoostNederland: Een break-outanalyse: Bijdrage in het multidisciplinair onderzoek naar de relatie tussen aardbevingen en gaswinning. Vrije Universiteit, Amsterdam.
- Segall, P.L., Fitzgerald, S.D., 1998. A note on induced stress changes in hydrocarbon and geothermal reservoirs. *Tectonophysics* 289, 117.
- Shapiro, S.A., Dinske, C., Langenbruch, C., Wenzel, F., 2010, March. Seismogenic index and magnitude probability of earthquakes induced during reservoir fluid stimulations. In: *The Leading Edge*, pp. 304.
- Soltanzadeh, H., Hawkes, C.D., 2008. Semi-analytical models for stress change and fault reactivation induced by reservoir production and injection. *J. Petrol. Sci. Eng.* 60, 71.
- Terzaghi, K., 1943. *Theoretical Soil Mechanics*. J. Wiley, New York.
- TNO-NITG, 2004. *Geological Atlas of the Subsurface of the Netherlands-onshore*. Netherlands Institute of Applied Geoscience TNO, Utrecht, pp. 104.
- Van Eijs, R.M.H.E., Mulders, F.M.M., Nepveu, M., Kenter, C.J., Scheffers, B.C., 2006. Correlation between hydrocarbon reservoir properties and induced seismicity in the Netherlands. *Eng. Geol.* 84, 99.

- Van Thienen-Visser, K., Nepveu, M., Hettelaat, J., 2012. Deterministische hazard analyse voor geïnduceerde seismiciteit in Nederland (No. R10198). TNO, Utrecht (Update seismic hazard) http://www.nlog.nl/resources/Seismic_Risk/2012%2025%2006-%20TNO%20technical%20rapport%20seismic%20hazard-public.pdf
- Van Wees, J.D., Orlic, B., Van Eijs, R., Zijl, W., Jongerius, P., Schreppers, G.J., Cornu, T., 2003. Integrated 3D geomechanical modelling for deep subsurface deformation: a case study of tectonic and human-induced deformation in the eastern Netherlands. *Geol. Soc., Lond., Special Publ.* 212 (1), 313–328.
- Verweij, J.M., Simmelink, H.J., Underschultz, J., Witmans, N., 2012. Pressure and fluid dynamic characterisation of the Dutch subsurface. *Neth. J. Geosci.* 91 (4), 465–490.
- Warpinski, N.R., 2012. Measurements of hydraulic-fracture-induced seismicity in gas shales. In: SPE Production and Operations (August), pp. 240.
- Van Wees, J.D.V., Beekman, F., 2000. Lithosphere rheology during intraplate basin extension and inversion inferences from automated modeling of four basins in Western Europe. *Tectonophysics* 320, 219.
- Wiemer, S., 2001. A software package to analyze seismicity: ZMAP. *Seismol. Res. Lett.* 72, 373–382.
- Wong, T.E., Batjes, D.A.J., de Jager, J., 2007. *Geology of the Netherlands*. Royal Netherlands Academy of Arts and Sciences, Amsterdam.
- Worum, G., van Wees, J., Bada, G., van Balen, R.T., Cloetingh, S., Pagnier, H., 2004. Slip tendency analysis as a tool to constrain fault reactivation: a numerical approach applied to three-dimensional fault models in the Roer Valley Rift system (South-east Netherlands). *J. Geophys. Res.* 109, 02401.
- Zoback, M.D., Townend, J., 2001. Implications of hydrostatic pore pressures and high crustal strength for the deformation of intraplate lithosphere. *Tectonophysics* 336, 19.
- Zielke, O., Arrowsmith, J.R., 2008. Depth variation of coseismic stress drop explains bimodal earthquake magnitude-frequency distribution. *Geophys. Res. Lett.* 35 (L24301).